


Gliding tremors associated with the 26 second microseism in the Gulf of Guinea

Charlotte Bruland^{1,2}✉ & Celine Hadziioannou ¹

A location in the Gulf of Guinea, which emits monochromatic seismic waves at 26-second period, seemingly continuously, was identified in the 1960s. However, the origin of these seismic waves remains enigmatic to date. Here we use three-component data from two seismic arrays in Africa, as well as additional seismic data compiled from around the world, to investigate the tremors. We identify frequency glides accompanying the previously known 26 s microseism which start at the same frequency and originate in the same, fixed location in the Gulf of Guinea. The stable characteristics of the tremors, their low frequency range, the implied large spatial scale, and the decades-long timescales where this phenomenon seems to have been active, all point towards a gap in our understanding of long period oceanic and volcanic signals. Since tremor is an important tool to monitor volcanoes, understanding this phenomenon may affect future forecasting of volcanic activity.

¹Institute of Geophysics, Center for Earth System Research and Sustainability (CEN), Universität Hamburg, Hamburg, Germany. ²NORSAR, Gunnar Randers vei 25, 2007 Kjeller, Norway. ✉email: charlotte.bruland@norsar.no

The mystery of the 26 s microseism has been puzzling geophysicists for decades. This sustained seismic signal is detected globally, with a constrained source location, but no observations so far seem to bring us closer to understanding which physical mechanism is causing this enigmatic signal. Here we demonstrate that gliding frequencies associated with the 26 s source are also detected globally, start at the same frequency and originate in the same fixed location in the Gulf of Guinea.

The 26 s signal, with approximate coordinates (0,0), was discovered in the 1960s and is believed to be generated continuously, from a fixed location, since then^{1–4}. Still, the physical mechanism remains unclear. Oliver¹ described a dispersive storm lasting about 2 days, with decreasing periods from about 28 to 20 s. We interpret this to be the very first observation of the glide. Later it was shown that this peak at 26 s was actually a persistent part of the ambient noise spectrum^{2,5}. Several temporally persistent narrow-band signals have previously been located in the gulf, at 27 and 16 s^{1,4,6}. As the sources at 27 and 16 s are located close to the Cameroon volcanic line, magmatic origin has been proposed. However, there are no known volcanoes in the area of the Gulf where the 26 s source is located⁴. Uncovering the physical mechanism behind the frequency glides presented here, and their connection to the 26 s source, might help put constraints on the source mechanism behind the seismic signals in the Gulf of Guinea.

Usually, such sustained seismic signals are linked to volcanic activity, called volcanic tremor⁷. Nevertheless, various natural sources can generate gliding tremor, such as hydrothermal systems^{8,9}, icebergs¹⁰, glaciers¹¹, microtsunamis¹², landslides, avalanches¹³ and swells¹⁴. Artificial sources, such as trains¹⁵ and helicopters¹⁶, can also produce harmonic gliding tremor, similar to what is observed at active volcanoes.

Other gliding tremor observations, however, typically have higher frequencies or shorter duration than the frequency gliding that we observe, and are only detected at short distances from the source. Tremors with characteristics such as those in the Gulf of Guinea have previously not been reported, and cannot be explained by known volcanic or oceanic mechanisms. In this study, we aim to constrain the mechanism of the glides.

Seismic data used in this study

To study the glide episodes, we use three-component data from two seismic arrays in Africa; the Morocco-Muenster array (MM), a temporary array located in Morocco (2011–2012)¹⁷, and the temporary installation Broadband Seismic Investigation of the Cameroon Volcanic Line (CVL)¹⁸ (2006). The locations and array configurations are shown in Fig. 1.

We also use available data from the permanent three-component broadband station TAM in Algeria from the global seismological network GEOSCOPE (G)¹⁹ (Fig. 1c) as well as other seismic stations (see Supplementary Table 1)^{19–22}.

Results

Gliding frequencies associated with the 26 s microseism. Seismic observations reveal the presence of very long period frequency glides on broadband 3-component stations close to the Gulf of Guinea. Figure 2 shows an example of such frequency glides from vertical component data from a station in Cameroon (station CM09 from the CVL array Fig. 1d) in May 2006. The gliding is a very narrow band and has an unusually long duration, up to several days. The frequency always glides up, from low frequency to higher frequencies. Closer inspection shows that the tremor starts at the same frequency as the 26 s microseism.

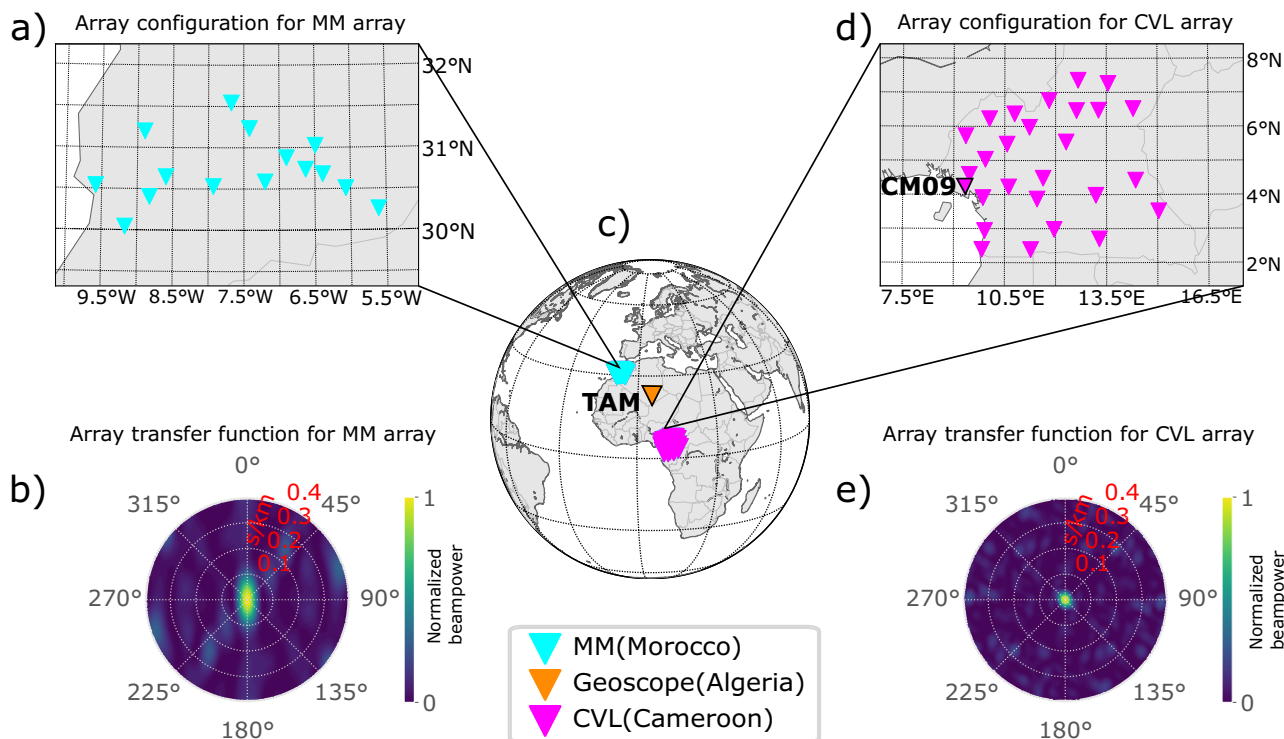


Fig. 1 Seismic stations used in this study. **a** Array configuration for the MM array (Morocco) consisting of 15 stations used for beamforming. **b** Beam power in the case of a single monochromatic plane wave coming from right below the array for the MM array. **c** Locations for seismic stations used in this study. **d** Array geometry for the part of the CVL array (Cameroon) comprised of 27 stations used for beamforming and beam power in the case of a single monochromatic plane wave coming from right below the array for the geometry given in **(e)**. The station's TAM and CM09 are used for spectral analysis. TAM is labeled and shown with an orange triangle with a black border **(c)**. CM09 is labeled and shown with a pink triangle with a black border in the CVL array in **(d)**.

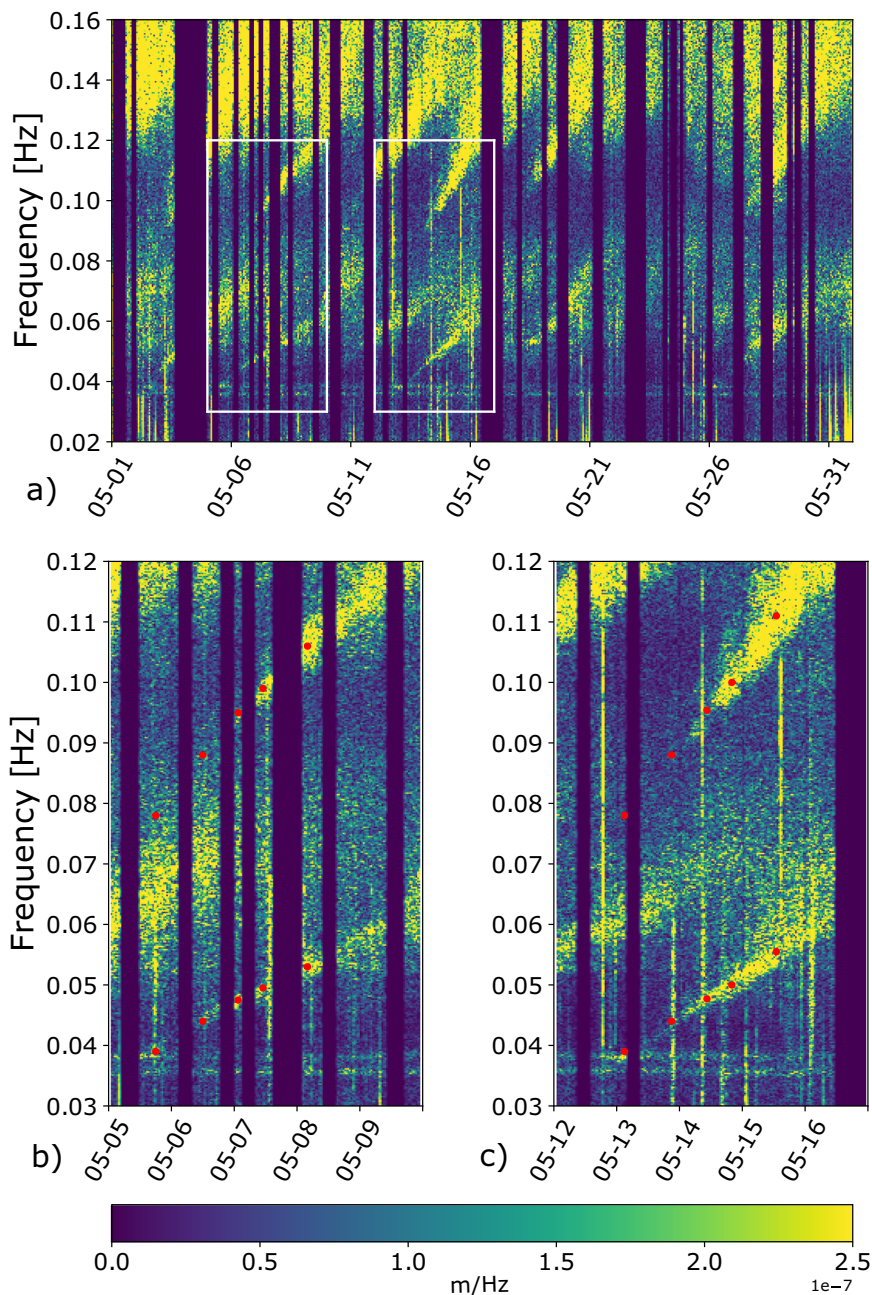


Fig. 2 Harmonic frequency gliding on vertical component data from CM09 in Cameroon in May 2006. **a** White boxes mark the glides starting May 5 and 13 shown in **(b)** and **(c)**. The lower set of red dots corresponds to the picked slope and the top red dots indicate the frequency of the overtone calculated from two times the fundamental frequency. The gliding starts at 0.038 Hz (26 s). We also see two persistent narrow-band tremors at 0.036 and 0.038 Hz, reported by Oliver¹ and Xia et al.⁴ respectively. The spectrogram is computed using a window length of 2 h and an overlap equal to 0.9.

Another remarkable observation is the linearity of the glides, as the frequency changes almost linearly from 0.038 Hz to at least 0.05 Hz. At this point, the primary ocean microseism drowns out the glide signal, and it can no longer be detected. The glides are harmonic, with a first visible fundamental frequency and an overtone with regular harmonic spacing, which appears to be maintained throughout the gliding episode. Both single glides and groups of glides are observed.

Inspecting seismic data from 10 consecutive years (2004–2013) on TAM (Fig. 1c) shows that the frequency gliding is caused by a long-lived and ongoing process. Given that the 26 s microseism has been active since at least the 1960s¹, and the glides are observed also on data from 1991 (Supplementary

Figs. 1 and 2), we infer that both phenomena have been active for decades.

Using 12, particularly clean and energetic glides, we compare the slopes from the given time period from the permanent broadband station TAM (Fig. 1c), which tells us that the majority of the glides have similar slopes (Fig. 3). This, together with the similar duration, points towards a common non-destructive physical process responsible for the seismic energy. The slope does not change depending on the distance traveled, so the frequency change is likely due to changes in the source. A burst in the seismic energy of the 26 s microseism often precedes the glide and continues after the glide has moved to higher frequencies, which supports a connection between the

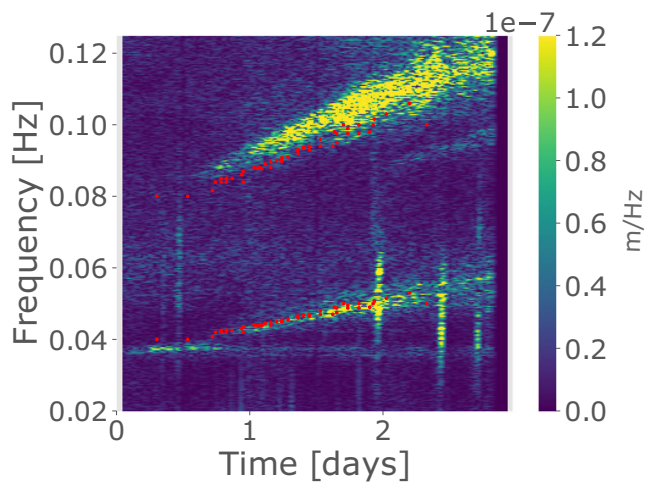


Fig. 3 Repeated gliding tremor. Slopes from 12 frequency glides detected on TAM from 2004 to 2013 are presented by the lower set of red dots. The glides exhibit a similar slope and are repeatable. We use the velocity (3.7 km s^{-1}) and the backazimuth (152 degrees) obtained from beamforming to delay and sum the traces from the stations of the Morocco array to enhance the gliding tremor on 2012-07-30 and compute the spectrogram of the resulting stacked waveform for 2 h windows with 0.9 overlap. The slopes from TAM match well with the slope from the glide detected in Morocco, and the 26 s signal is amplified with the glide. The top red dots show at what frequency we expect the overtone calculated from two times the picked fundamental frequency (lower red dots). The overtone is consistently higher than what is predicted for regular harmonic spacing, both for the glide detected on TAM and the Morocco array, so the harmonic spacing changes over time.

phenomena driving the glides and the 26 s source. Despite the change in the frequency of the gliding tremor, the frequency of the continuous signal remains stable. Hence, we have stable and varying spectral peaks generated simultaneously, likely emerging from the same, or coupled physical processes.

Although the glides are the most prominent on seismic stations close to the Gulf of Guinea, the more energetic glides are also observed on quiet stations globally (Fig. 4, Supplementary Table 1). Data from seismic stations globally exhibit the same 26 s spectral peak and simultaneous gliding. This is similar to the 26 s microseism, which occasionally grows strong enough to be detected globally. Such energetic bursts in the 26 s band usually last for hours and are as strong as a magnitude 5 earthquake⁴. To further constrain the relationship between the gliding and the continuous, 26 s signal, we use seismic array processing.

Are the two phenomena spatially connected? We constrain the source region by applying three-component beamforming^{23–25} using a temporary seismic array in Morocco (MM) and the temporary installation of Broadband Seismic Investigation of the Cameroon Volcanic Line (CVL)¹⁸ (Supplementary Table 2). We perform beamforming on 500 s time windows, with slowness increments of 0.02 s/km and 2-degree steps for back azimuth for both Rayleigh and Love waves.

The beam power spectral density is normalized by the average station power spectral density of all components. The beam power is calculated for 10-h intervals at frequency $f = 0.038 \pm 0.001 \text{ Hz}$ and $f = 0.048 \pm 0.001 \text{ Hz}$, in order to differentiate between the glides and the 26 s microseism. For each beamformer output, the back azimuth corresponding to the maximum beam power is selected. The back projection along the estimated back azimuth points towards the Gulf of Guinea (Fig. 5), and this dominant

direction is equal for all 5 glides investigated from 2011 and 2012 from the Morocco array and the 3 glides on the Cameroon array from May 2006 (Supplementary Table 3). On the Morocco array, both Love and Rayleigh waves are detected for both signals, arriving from the same direction. In addition, there is no significant change in direction over the course of a glide (Fig. 6a). From this it follows that the signals are coming from a fixed location and that this location is temporally stable over the two years investigated with array analysis. We also determine that this location is consistent with that found for the 26 s microseism^{2–4} within the resolution of the beamforming. Consequently, we infer that the two phenomena share a common source area.

Physical mechanisms for gliding tremor

Based on our observations, the physical mechanism generating the frequency glides should fulfill the following criteria: it should be repeatable, implying either reversibility or a recharge mechanism; it should be capable of continuously outputting energy for at least 60 years; it should be energetic enough to be observed globally; it should have a fixed location; and finally, since the glides are connected to the monochromatic, 26 s microseism in frequency, time and space, the mechanism should be able to generate both stable and varying frequency peaks simultaneously. In the following, we consider both volcanic and oceanic source mechanisms.

Volcanic gliding tremor. Volcanic tremor is usually only recorded near the volcano, but can occasionally be observed globally²⁶. In addition, volcanic tremor typically occurs at much higher frequencies (1–5 Hz) and shorter duration (minutes) than the Gulf of Guinea gliding tremor²⁷. Still, long-lasting and long-period gliding tremor is detected at multiple locations^{28–30}. However, in these cases, the change in frequency is irregular, not repeatable, with alternating frequency increases and decreases, in contrast to our linear upward glides. Whenever repeating upward gliding is observed, it is usually associated with volcanic eruptions^{31–33} and is typically explained by a fluid-filled resonator or a regular repeated source.

Resonating fluid-filled magma pathways. A fluid-filled resonator, for example, gas resonating in a conduit can explain the occurrence of harmonic tremor^{34,35} with the fundamental frequency (f_0) given by: $f_0 = c/2L$, where c is the acoustic velocity in the resonating medium, and L is the length of the crack or conduit³⁶. Very long period (15 s) tremor at Mayotte, which was also observed globally, was interpreted as the resonance of a 10–15 km reservoir²⁶. In order to obtain a fundamental frequency of 0.038 Hz, we would expect the resonator length to be even larger. Due to the large dimensions required for such a resonator and the need for a process that can reset quickly in a repeatable manner, we conclude that the frequency glides are not likely due to changes in resonator length alone.

An alternative to geometric changes in the conduit is a change in the fluid properties, essentially changing the velocity. Small changes in gas fraction can produce large velocity changes³³, and hence changes in the resonator frequency, which is easily reversible and can therefore accommodate the observed repeatability of the glides. For example, new material being injected into the conduit can produce repeated narrow-band gliding tremors with a roughly linear increase in frequency, which is observed at underwater volcanoes prior to eruptions³⁷.

The injected material increases the gas content, which in turn decreases as the gas is released from the vent, thus changing the wave velocity in the magma^{37,38}. For a hydrothermal system, with lower fluid velocities, low-frequency tremor could be realized for shorter resonator lengths.

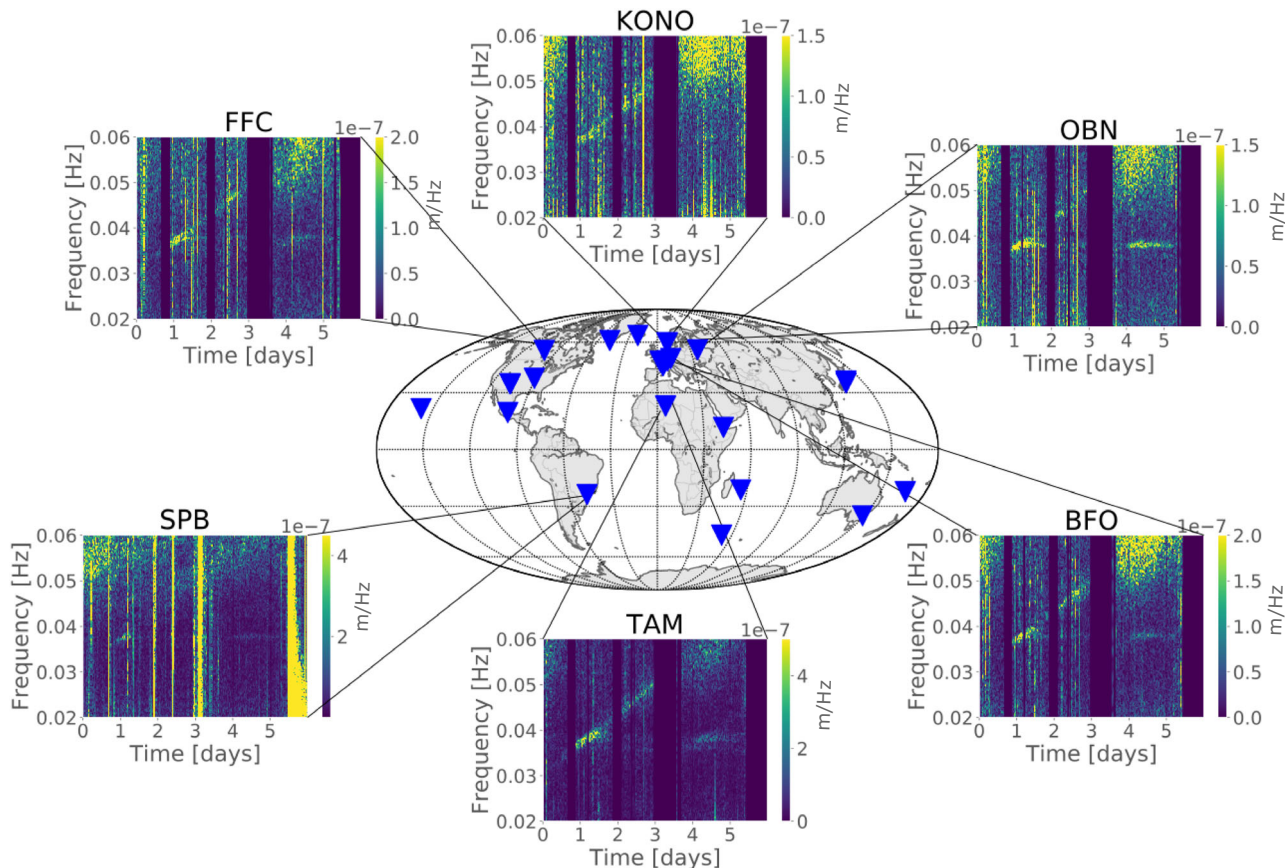


Fig. 4 Global observations of burst and gliding tremor. Gliding tremor is detected on seismic stations globally (Supplementary Table 1). Spectrograms for TAM, BFO, OBN, KONO, FFC, and SPB are shown. The spectrograms are computed with a window length of 60 min and 50% overlap starting 2013-04-11 to 2013-04-17.

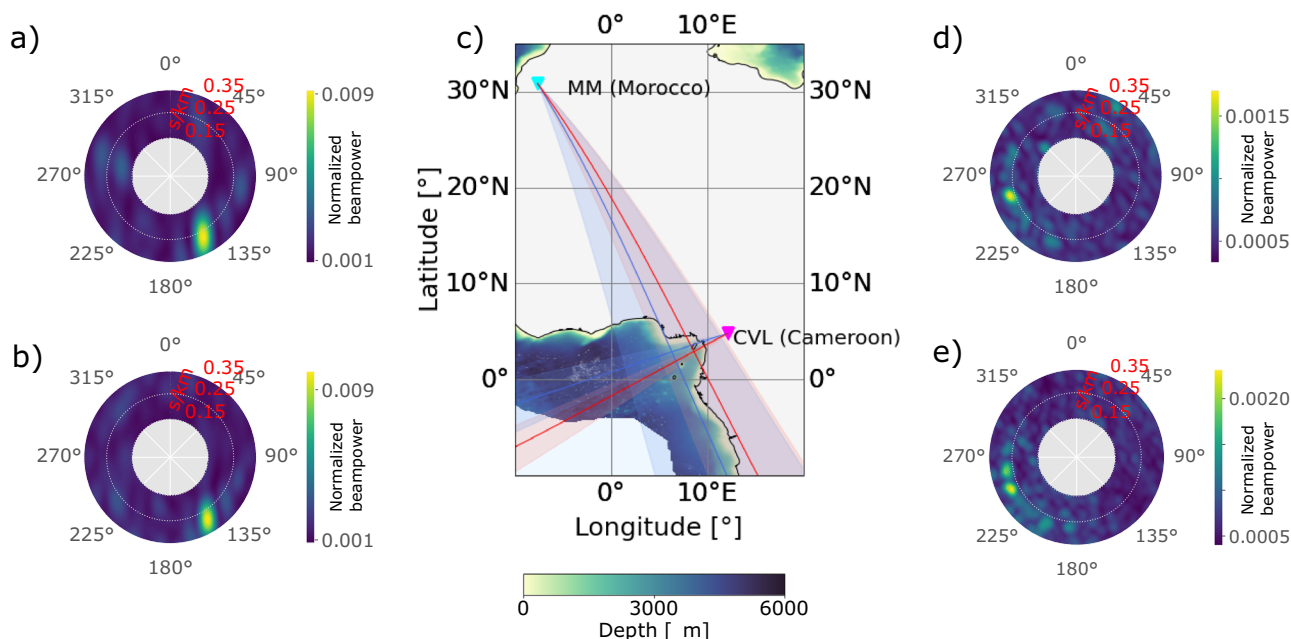


Fig. 5 Projected back azimuth for the glide and 26 s source. The beam power as a function of slowness and back azimuth for the Rayleigh wave for the 26 s (blue) and the glide (red) is shown in (a), (d) and (b), (e), respectively. c The back azimuth corresponding to the maximum beam power from the beamforming outputs towards the Gulf of Guinea for the 26 s microseism and the glide, with uncertainties calculated from half of the maximum beam power shown with the bathymetry in the gulf.

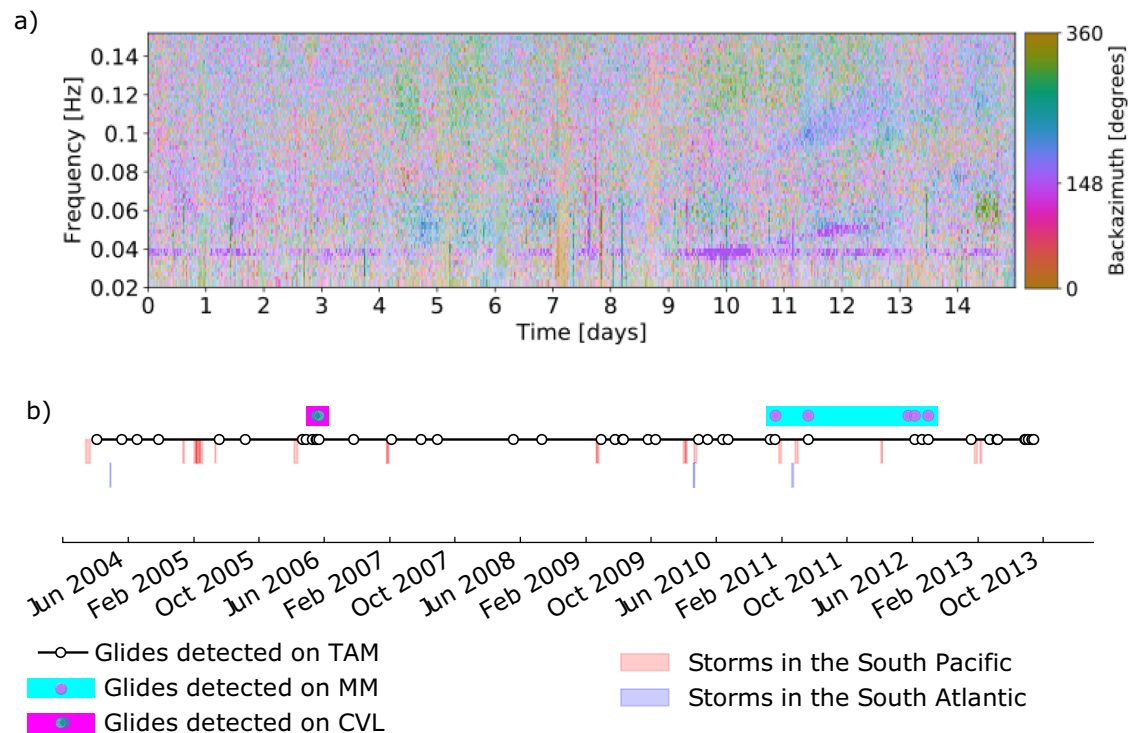


Fig. 6 Gliding tremors, storms and locations. **a** Beam power and back azimuth in frequency and time for stacked beamforming results for 5 glides detected on the Morocco array (2011–2012), starting 10 days before the start of the glide. To emphasize the areas where the most detectable signal is present, we placed a transparency mask over the back azimuth–frequency plot, with full transparency for the highest beam powers and less transparency for the lowest beam powers. **b** The distribution of frequency glides over 10 years (2004–2013) is shown. The glides detected on the MM array and CVL array are displayed above, with the back azimuth obtained from beamforming, 148 degrees, and about 244 degrees, respectively. Below the storm occurrence in the South Pacific and South Atlantic is presented.

Regular repeated source. Repeated sources, spaced regularly in time, such as earthquakes or repetitive pressure transients, are also known to produce a harmonic-like tremor^{31–33}. As the pulses move closer together, the harmonic tremor glides to higher frequencies. When the pulse spacing drifts further apart, the tremor glides to lower frequencies. To fit our observations, the trigger frequency needs to gradually change from 0.038 to 0.05 Hz, with a lag time between the pulses equal to the inverse of the frequency. Whether this repeated source is earthquakes, pressure transients, it is difficult to reproduce the same conditions to have the same trigger frequency and the same change in trigger frequency over decades. This would require an additional mechanism to control the frequency. Still, both mechanisms described above could potentially explain our repeatable, upward gliding tremor as well as the harmonic overtones, but we need an explanation for the simultaneous, monofrequent 26 s signal as well. To explain the two phenomena, one tremor mechanism might not be sufficient.

Combination of simultaneous mechanisms. The continuous, stable peak at 26 s that we observe coming from the Gulf of Guinea could be a result of a large, magmatic or hydrothermal system, such as a reservoir, continuously degassing, exciting the system into resonance, while the frequency glides could be related to the gas escaping through a narrow conduit.

Lesage et al.³³ proposed a “clarinet” model to explain the gliding tremor observed at Arenal, Costa Rica, consisting of a conduit closed off by a fractured plug. Harmonic tremor is produced by repetitive pressure pulses, with a repeat period that stabilizes through feedback with the resonance frequency of the conduit, due to the pressure variations driven by standing waves in the conduit.

Such a feedback mechanism could explain why our glides start at the same frequency as the 26 s microseism, with the source of the glide either connected to or controlled by the 26 s source. To explain the 26 s source, which has had stable properties for decades, we need a magmatic or hydrothermal system with a resonance period of 26 s, like a channel or reservoir, that is set into resonance by an internal mechanism such as boiling groundwater or gas release. The upward glide points towards gas release, so the system would be sealed off by a plug that acts as a valve through which gas can escape intermittently.

With the help of satellite data (sea surface height from Jason-3, Sentinel-3A, HY-2A, Saral/AltiKa, Cryosat-2, Jason-2, Jason-1, T/P, ENVISAT, GFO, ERS1/2³⁹ and sea surface temperature from OSTIA SST analysis combining satellite data from the GHRSSST project and in-situ observations to determine sea surface temperature⁴⁰) we searched for evidence of sea surface disturbance by rising bubbles at the time of several glides and did not detect anything. Therefore we look into oceanic mechanisms.

Ocean generated mechanisms. Linear gliding features in seismic spectrograms can be observed as a result of remote storms over the oceans. These storms generate ocean gravity waves, typically with periods ranging from 3 to 20 s¹⁴. When the dispersed ocean waves arrive at the coast, the low-frequency waves reach the shore first, followed by increasingly higher-frequency waves⁴¹. As the swell couples into the seafloor and generate seismic waves, it produces a characteristic fan-like shape in seismic spectrograms, broadening towards higher frequencies, with a duration of up to a few days⁴². The slope of the resulting shape gives an estimate of the distance to the storm¹⁴. Applying this to our glide on May 13th, we estimate a distance over 11,200 km between storm and coast, which would

place the storm in the South Pacific, south of the typical hurricane track latitudes⁴³. The strong repeatability in our glide slopes would imply repeated storms at the same distance if they were all to be explained by storm-generated seismic waves. Moreover, as the frequency of the ocean waves generated by a storm is determined by the wind speed⁴⁴, intense storms with sustained wind speeds exceeding 20 m s^{-1} would be necessary to explain the low-frequency onset of our glides¹⁴. A comparison to meteorological data^{43,45,46} does not show any correlation between storm occurrence and glide dates (Fig. 6). Here, global hurricane databases are considered, since no database containing all low-frequency swell events was available.

Distant storms would also not explain why the gliding appears to have a very similar low-frequency onset, starting at approximately the same frequency as the 26 s microseism. For the continuous tremor to be explained by ocean waves, we would need 26 or 52 s waves continuously in the gulf. Since such low-frequency ocean waves are only associated with the most energetic storms, we conclude that a fully oceanic origin for the phenomena in the Gulf of Guinea is very unlikely. Although we cannot explain the 26 s source with oceanic mechanisms, the phenomena could be explained by a combination of volcanic and oceanic mechanisms. If the glides are the signature of storm-generated seismic waves, Chen et al.⁴⁷ suggest that the bursts in the 26 s tremor accompanying the frequency glides relate to ocean waves arriving in the gulf from the South Pacific which pass over the resonator and amplify the system. Hence, we would have a hydrothermal system that is modulated by ocean microseisms.

Our suggested mechanisms. We propose two possible mechanisms: (1) A hydrothermal system consisting of a layered structure or channel that is set into resonance by an internal mechanism such as boiling groundwater or gas release. The channel is sealed off by a fractured plug that acts as a valve through which gas can escape intermittently, thereby producing pressure pulses with a repetition period stabilized by the resonance of the channel. (2) A hydrothermal system modulated by storm-generated ocean waves passing overhead.

Conclusions

Since the source is hidden from view and there are no known surface manifestations such as gas bubbles, sea surface disturbances or thermal anomalies, it is difficult to confirm that degassing occurs at depth. There are also no buoys to confirm 26 or 52 s ocean waves in the Gulf. Although the discovery of the frequency glides provides us with another piece of the puzzle surrounding the 26 s microseism, many questions still remain unanswered, and will likely remain so until we have additional, in-situ observations. With the established volcanic and oceanic models for tremor, it remains difficult to fully explain the seismic signals in terms of repeatability, strength and low frequency, nor do they account for the decade-long, stable release of energy. An additional complication is finding an explanation for both the glides and the continuous 26 s signal simultaneously. Regardless, the nature of the Gulf of Guinea tremors forces us to broaden our thinking about the mechanisms and systems causing gliding tremors, and about the mysterious signals the Earth produces.

Methods

Preprocessing. The data used for beamforming is processed in 1-day segments. First, the daily traces are corrected for instrument response and resampled to 1 Hz. Then, the mean and trend are removed, and the traces are band-pass filtered between 0.01 and 0.06 Hz.

To remove the influence of earthquakes, we use a catalog of global earthquakes. The catalog includes global earthquakes above $M = 5.5$ and is based on the ISC bulletin⁴⁸. Following the approach of Tanimoto et al.⁴⁹, after each earthquake, we removed a section of the signal. The length of the removed section was adapted to the magnitude of the earthquake, removing particularly long time windows after

high-magnitude earthquakes to account for the excitation of the normal modes of the Earth. We remove 6 h for earthquakes between magnitude 5.5 and 6, starting at the time of the earthquake. For magnitudes up to 8, 12 h are removed, above magnitude 8 we remove 24 h, and for earthquakes larger than magnitude 9 we remove 36 h.

To further eliminate the effects of smaller, local earthquakes and spikes in the data, an STA/LTA trigger is also included with STA = 500 s and LTA = 24 h. All data processing is done with ObsPy^{50–52}.

3-component beamforming. We use a three-component beamforming method²³ in the frequency domain to separate between differently polarized waves and obtain estimates of beam power, the direction of arrival (back azimuth), and slowness of the incoming coherent signals. The method has previously been applied to ambient noise by Riahi et al., Juretzek et al.^{24,25,53} and Löer et al.⁵⁴. For a detailed description of the method, we refer to Riahi et al.²⁴.

We perform beamforming on 500 s time windows, with slowness increments of 0.02 s/km and 2° steps for back azimuth for both Rayleigh and Love waves.

The beam power spectral density is normalized by the average station power spectral density of all components. The beam power is calculated for 10-h-intervals at frequency $f = 0.038 \pm 0.001 \text{ Hz}$ and $f = 0.048 \pm 0.001 \text{ Hz}$, in order to separate between the glides and the 26 s microseism. For each beamformer output, the back azimuth corresponding to the maximum beam power is selected.

Array configuration and limitations. To evaluate the performance of the Morocco array¹⁷, we evaluate the beam power in the case of a single monochromatic plane wave coming from right below the array. The resulting beam power is called the array transfer function and is affected by a number of stations, spatial configuration and array aperture. The main lobe of the transfer function represents the power distribution in the true arrival direction of the signal, while the side lobes are the energy contribution at other slownesses. An ideal transfer function thus has a narrow main lobe, with low power contribution from the side lobes⁵⁵. Figure 1b and e show the resolution capability of the Morocco array and the Cameroon array at a frequency of 0.038 Hz for the array geometry shown in Fig. 1a and d. The array transfer function slightly differs at different frequencies, but the effect is not strong enough to affect our results.

Data availability

All data used in this work is available through FDSN. We use data from the permanent seismic stations described in Supplementary Table 1^{19–22}. In addition, we use available data from the temporary installation Broadband Seismic Investigation of the Cameroon Volcanic Line (CVL)¹⁸ and a temporary array located in Morocco from 2011 to 2013¹⁷ described in Supplementary Table 2.

Code availability

The analysis was done using the ObsPy⁵¹, Numpy⁵⁶ and SciPy⁵⁷ libraries. Figures were created using matplotlib⁵⁸. Specific analysis scripts are available upon request.

Received: 7 February 2022; Accepted: 5 May 2023;

Published online: 23 May 2023

References

- Oliver, J. A worldwide storm of microseisms with periods of about 27 seconds. *Bull. Seismol. Soc. Am.* **52**, 507–517 (1962).
- Holcomb, L. G. Microseisms: a twenty-six-second spectral line in long-period earth motion. *Bull. Seismol. Soc. Am.* **70**, 1055–1070 (1980).
- Shapiro, N. M., Ritzwoller, M. & Bensen, G. Source location of the 26 sec microseism from cross-correlations of ambient seismic noise. *Geophys. Res. Lett.* **33**, L18310 (2006).
- Xia, Y., Ni, S. & Zeng, X. Twin enigmatic microseismic sources in the Gulf of Guinea observed on intercontinental seismic stations. *Geophys. J. Int.* **194**, 362–366 (2013).
- Holcomb, L. G. Spectral structure in the Earth's microseismic background between 20 and 40 seconds. *Bull. Seismol. Soc. Am.* **88**, 744–757 (1998).
- Xia, Y. & Chen, X. Observation of a new long-period (16-s) persistent tremor originating in the Gulf of Guinea. *Geophys. Res. Lett.* **47**, e2020GL088137 (2020).
- Konstantinou, K. I. & Schlindwein, V. Nature, wavefield properties and source mechanism of volcanic tremor: a review. *J. Volcanol. Geotherm. Res.* **119**, 161–187 (2003).
- Nayak, A., Manga, M., Hurwitz, S., Namiki, A. & Dawson, P. B. Origin and properties of hydrothermal tremor at Lone Star Geyser, Yellowstone National Park, USA. *J. Geophys. Res.: Solid Earth* **125**, e2020JB019711 (2020).
- Franek, P., Mienert, J., Buenz, S. & Géli, L. Character of seismic motion at a location of a gas hydrate-bearing mud volcano on the SW Barents Sea margin. *J. Geophys. Res.: Solid Earth* **119**, 6159–6177 (2014).

10. MacAyeal, D., Okal, E., Aster, R. & Bassis, J. Seismic and hydroacoustic tremor generated by colliding icebergs. *J. Geophys. Res.: Earth Surf.* **113**, F03011 (2008).
11. Helmstetter, A., Moreau, L., Nicolas, B., Comon, P. & Gay, M. Intermediate-depth icequakes and harmonic tremor in an Alpine glacier (Glacier d'Argentière, France): evidence for hydraulic fracturing? *J. Geophys. Res.: Earth Surf.* **120**, 402–416 (2015).
12. MacAyeal, D. R., Okal, E. A., Aster, R. C. & Bassis, J. N. Seismic observations of glaciogenic ocean waves (micro-tsunamis) on icebergs and ice shelves. *J. Glaciol.* **55**, 193–206 (2009).
13. Suriñach Cornet, E. et al. Seismic detection and characterization of landslides and other mass movements. *Nat. Hazards Earth Syst. Sci.* **5**, 791–798 (2005).
14. Bromirski, P. D. & Duennebier, F. K. The near-coastal microseism spectrum: spatial and temporal wave climate relationships. *J. Geophys. Res.: Solid Earth* **107**, ESE-5 (2002).
15. Fuchs, F. & Bokelmann, G. Equidistant spectral lines in train vibrations. *Seismol. Res. Lett.* **89**, 56–66 (2018).
16. Eibl, E. P., Lokmer, I., Bean, C. J., Akerlie, E. & Vogtjörð, K. S. Helicopter vs. volcanic tremor: characteristic features of seismic harmonic tremor on volcanoes. *J. Volcanol. Geotherm. Res.* **304**, 108–117 (2015).
17. Thomas, C. Morocco-Muenster https://doi.org/10.7914/SN/3D_2010 (2010).
18. Douglas Wiens, A. N. Broadband seismic investigation of the Cameroon volcanic line https://doi.org/10.7914/SN/XB_2005 (2005).
19. Institut De Physique Du Globe De Paris (IPGP) & Ecole Et Observatoire Des Sciences De La Terre De Strasbourg (EOST). GEOSCOPE, French Global Network of broadband seismic stations <https://doi.org/10.18715/GEOSCOPE.G> (1982).
20. Albuquerque Seismological Laboratory/USGS. Global seismograph network (gsn-iris/usgs) <https://doi.org/10.7914/SN/IU> (2014).
21. Scripps Institution of Oceanography. Global seismograph network—iris/ida. <https://doi.org/10.7914/SN/II> (1986).
22. Federal Institute for Geosciences and Natural Resources. German Regional Seismic Network (GRSN) <https://doi.org/10.25928/MBX6-HR74> (1976).
23. Esmersoy, C., Cormier, V. & Toksoz, M. Three-component array processing. In *The VELA Program. A Twenty-Five Year Review of Basic Research*. (ed. Kerr, A. U.) Vol. 78, 1725–1743 (Executive Graphic Services, 1985).
24. Riahi, N., Bokelmann, G., Sala, P. & Saenger, E. H. Time-lapse analysis of ambient surface wave anisotropy: a three-component array study above an underground gas storage. *J. Geophys. Res.: Solid Earth* **118**, 5339–5351 (2013).
25. Juretzek, C. & Hadziioannou, C. Where do ocean microseisms come from? A study of Love-to-Rayleigh wave ratios. *J. Geophys. Res.: Solid Earth* **121**, 6741–6756 (2016).
26. Cesca, S. et al. Drainage of a deep magma reservoir near Mayotte inferred from seismicity and deformation. *Nat. Geosci.* **13**, 87–93 (2020).
27. McNutt, S. R. Volcanic tremor. *Encycl. Earth Syst. Sci.* **4**, 417–425 (1992).
28. Hellweg, M. Physical models for the source of Lascar's harmonic tremor. *J. Volcanol. Geotherm. Res.* **101**, 183–198 (2000).
29. Dawson, P. B., Benitez, M., Chouet, B. A., Wilson, D. & Okubo, P. G. Monitoring very-long-period seismicity at Kilauea Volcano, Hawaii. *Geophys. Res. Lett.* **37**, L18306 (2010).
30. Kawano, Y. et al. Persistent long-period signals recorded by an OBS Array in the Western-Central Pacific: activity of Ambrym Volcano in Vanuatu. *Geophys. Res. Lett.* **47**, e2020GL089108 (2020).
31. Hotovec, A. J., Prejean, S. G., Vidale, J. E. & Gomberg, J. Strongly gliding harmonic tremor during the 2009 eruption of Redoubt Volcano. *J. Volcanol. Geotherm. Res.* **259**, 89–99 (2013).
32. Lees, J. M., Gordeev, E. I. & Ripepe, M. Explosions and periodic tremor at Karymsky volcano, Kamchatka, Russia. *Geophys. J. Int.* **158**, 1151–1167 (2004).
33. Lesage, P., Mora, M. M., Alvarado, G. E., Pacheco, J. & Métaixian, J.-P. Complex behavior and source model of the tremor at Arenal volcano, Costa Rica. *J. Volcanol. Geotherm. Res.* **157**, 49–59 (2006).
34. Schlindwein, V., Wassermann, J. & Scherbaum, F. Spectral analysis of harmonic tremor signals at Mt. Semeru volcano, Indonesia. *Geophys. Res. Lett.* **22**, 1685–1688 (1995).
35. Kawakatsu, H. et al. Aso94: Aso seismic observation with broadband instruments. *J. Volcanol. Geotherm. Res.* **101**, 129–154 (2000).
36. Hagerty, M., Schwartz, S. Y., Garces, M. & Protti, M. Analysis of seismic and acoustic observations at Arenal Volcano, Costa Rica, 1995–1997. *J. Volcanol. Geotherm. Res.* **101**, 27–65 (2000).
37. Searcy, C. Seismicity associated with the May 2010 eruption of South Sarigan Seamount, northern Mariana Islands. *Seismol. Res. Lett.* **84**, 1055–1061 (2013).
38. Dziak, R. P. & Fox, C. G. Evidence of harmonic tremor from a submarine volcano detected across the Pacific Ocean basin. *J. Geophys. Res. Solid Earth* **107**, ESE-1 (2002).
39. CLS (France). Global ocean gridded L4 sea surface heights and derived variables reprocessed (1993-ongoing) <https://doi.org/10.48670/moi-00148> (2012).
40. CNR (Italy). Global ocean OSTIA sea surface temperature and sea ice analysis <https://doi.org/10.48670/moi-00165> (2009).
41. Haubrich, R., Munk, W. & Snodgrass, F. Comparative spectra of microseisms and swell. *Bull. Seismol. Soc. Am.* **53**, 27–37 (1963).
42. Chevrot, S. et al. Source locations of secondary microseisms in western Europe: evidence for both coastal and pelagic sources. *J. Geophys. Res. Solid Earth* **112**, B11301 (2007).
43. Knapp, K. R. et al. Ncdc international best track archive for climate stewardship (ibtracs) project, version 3. <https://data.noaa.gov/dataset/ncdc-international-best-track-archive-forclimate-stewardship-ibtracs-project-version-3> (2010).
44. Pierson Jr, W. J. & Moskowitz, L. A proposed spectral form for fully developed wind seas based on the similarity theory of a saikaigorodskii. *J. Geophys. Res.* **69**, 5181–5190 (1964).
45. Knapp, K. R., Kruk, M. C., Levinson, D. H., Diamond, H. J. & Neumann, C. J. The international best track archive for climate stewardship (ibtracs) unifying tropical cyclone data. *Bull. Am. Meteorol. Soc.* **91**, 363–376 (2010).
46. Landsea, C. W. & Franklin, J. L. Atlantic hurricane database uncertainty and presentation of a new database format. *Mon. Weather Rev.* **141**, 3576–3592 (2013).
47. Chen, Y., Xie, J. & Ni, S. Generation mechanism of the 26 s and 28 s tremors in the Gulf of Guinea from statistical analysis of magnitudes and event intervals. *Earth Planet. Sci. Lett.* **578**, 117334 (2022).
48. ISC On-line Bulletin. International Seismological Centre (2021). <https://doi.org/10.31905/D808B830>.
49. Tanimoto, T., Lin, C.-J., Hadziioannou, C., Igel, H. & Vernon, F. Estimate of Rayleigh-to-Love wave ratio in the secondary microseism by a small array at Piñon Flat Observatory, California. *Geophys. Res. Lett.* **43**, 11–173 (2016).
50. Beyreuther, M. et al. ObsPy: a Python toolbox for seismology. *Seismol. Res. Lett.* **81**, 530–533 (2010).
51. Krischer, L. et al. Obspy: a bridge for seismology into the scientific Python ecosystem. *Comput. Sci. Discov.* **8**, 014003 (2015).
52. Team, T. O. D. Obspy 1.2.0 <https://doi.org/10.5281/zenodo.3674646> (2020).
53. Juretzek, C. & Hadziioannou, C. Linking source region and ocean wave parameters with the observed primary microseismic noise. *Geophys. J. Int.* **211**, 1640–1654 (2017).
54. Löer, K., Riahi, N. & Saenger, E. H. Three-component ambient noise beamforming in the Parkfield area. *Geophys. J. Int.* **213**, 1478–1491 (2018).
55. Nakata, N., Gualtieri, L., & Fichtner, A. (Eds.). *Seismic Ambient Noise*. 30–68 (Cambridge University Press, Cambridge, 2019). <https://doi.org/10.1017/9781108264808>.
56. Harris, C. R. et al. Array programming with numpy. *Nature* **585**, 357–362 (2020).
57. Virtanen, P. et al. Scipy 1.0: fundamental algorithms for scientific computing in Python. *Nat. Methods* **17**, 261–272 (2020).
58. Hunter, J. D. Matplotlib: a 2d graphics environment. *Comput. Sci. Eng.* **9**, 90–95 (2007).

Acknowledgements

We are grateful to Éléonore Stutzmann, Lise Retailleau, Joachim Wassermann, Christoph Sens-Schönfelder, Torsten Dahm and Stephen McNutt for helpful discussions and comments. We would also like to thank Stefan Kern for assisting with satellite data. We thank the editors, as well as Victor Tsai and three anonymous reviewers for their comments, which helped improve the manuscript.

Author contributions

C.B. and C.H. contributed to the analysis, interpretation of results and preparation of the manuscript.

Funding

Open Access funding enabled and organized by Projekt DEAL.

Competing interests

The authors declare no competing interests.

Additional information

Supplementary information The online version contains supplementary material available at <https://doi.org/10.1038/s43247-023-00837-y>.

Correspondence and requests for materials should be addressed to Charlotte Bruland.

Peer review information *Communications Earth & Environment* thanks Victor Tsai and the other, anonymous, reviewer(s) for their contribution to the peer review of this work. Primary Handling Editors: Luca Dal Zilio, Joe Aslin and Clare Davis. A peer review file is available.

Reprints and permission information is available at <http://www.nature.com/reprints>

Publisher's note Springer Nature remains neutral with regard to jurisdictional claims in published maps and institutional affiliations.



Open Access This article is licensed under a Creative Commons Attribution 4.0 International License, which permits use, sharing, adaptation, distribution and reproduction in any medium or format, as long as you give appropriate credit to the original author(s) and the source, provide a link to the Creative Commons license, and indicate if changes were made. The images or other third party material in this article are included in the article's Creative Commons license, unless indicated otherwise in a credit line to the material. If material is not included in the article's Creative Commons license and your intended use is not permitted by statutory regulation or exceeds the permitted use, you will need to obtain permission directly from the copyright holder. To view a copy of this license, visit <http://creativecommons.org/licenses/by/4.0/>.

© The Author(s) 2023